Electronic Supporting Information

Reaction study of α-phase $NaYF_4$:Yb,Er generation via a tubular microreactor: Discovery of an efficient synthesis strategy

Di Liu, Yu Jing, Kai Wang,* Yundong Wang,* Guangsheng Luo

The State Key Lab of Chemical Engineering, Department of Chemical Engineering, Tsinghua University, Beijing 100084, China

*Corresponding author email: kaiwang@tsinghua.edu.cn; wangyd@tsinghua.edu.cn

Microreactor experiment

The microreactor platform is shown in Figure S1. The reactant solutions were fed by high pressure syringe pumps (PHD Ultra 70-3310C, Harvard Apparatus) and 50 mL stainless steel syringes. The self-made quartz reaction tube was in the oil bath, and it was connected to the perfluoroalkoxy alkanes (PFA) tubes with polyetheretherketone (PEEK) connectors. The oil bath temperature was monitored by the thermometer. The reaction product was collected in the glass bottle with the protection of nitrogen in balloon.

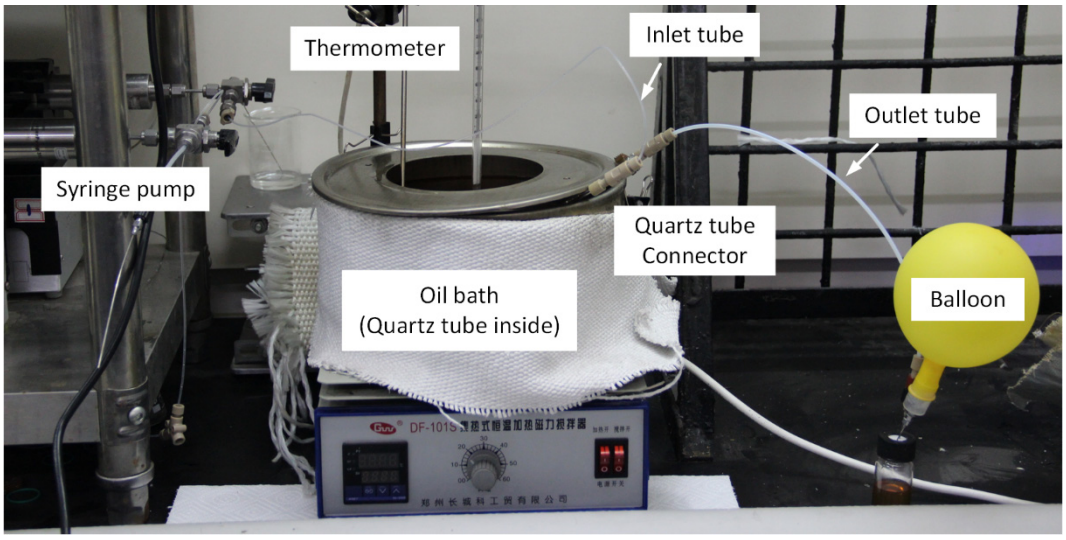

Figure S1. Picture of the microreactor platform

Computational fluid dynamics simulation

The microreactor has strong ability to control the reaction temperature owing to the rapid heat exchange with the environment. Fast heating and cooling of the solution were exhibited by computational fluid dynamics (CFD) simulation. Due to the low concentration of reactants, only the mixture of oleic acid and 1-octadecene (40%/60% volume fraction) was considered in the modes programed by COMSOL Multiphysics 4.3. The continuity equation, Naiver-Stokes equation and Diffusion-Convection equation for laminar flow were solved together, which are shown in Equations S1 to S4.

$$\nabla \cdot \mathbf{u} = 0 \tag{S1}$$

$$\rho \mathbf{u} \cdot \nabla \mathbf{u} = -\nabla p + \mu \nabla^2 \mathbf{u} \tag{S2}$$

$$\nabla \cdot \left(k_{\mathrm{q}} \nabla T_{\mathrm{q}} \right) = 0 \tag{S3}$$

$$\rho C_{\mathrm{p}} \mathbf{u} \cdot \nabla T_{\mathrm{s}} = \nabla \cdot \left(k \nabla T_{\mathrm{s}} \right) \tag{S4}$$

Here, $\mathbf{u}$ is the velocity vector, ρ is the solution density, μ is the solution dynamic viscosity, p is pressure, T_{q} is the quartz temperature, T_{s} is the solution temperature, k_{q} is the heat conductivity of quartz, k is the heat conductivity of solution, and C_{p} is the heat capacity of solution. Since the temperature is changed greatly, the variations of physical parameters were also considered in the program. The values of density, viscosity, heat conductivity and heat capacity were first collected from the Chemistry and Chemical Property Data Manual,[1] and then imported into the COMSOL program with regressions (Equations S5-S13). Since the density and viscosity of 1-octadecene at >40°C are not collected in the data book, we used the density and viscosity of octodecane for instead, and thus the CFD simulation just gave an evaluation of the temperature. The heat conductivity and capacity of 1-octadecene were self-measured with an NETZSCH instruments (LFA467 and DSC214).

$$\rho_{\mathrm{HOA}} = -0.0005 T_{\mathrm{s}}^2 - 0.3243 T_{\mathrm{s}} + 1028 \ (\mathrm{kg/m^3}) \tag{S5}$$

$$\rho_{\mathrm{OCT}} = -0.6656 T_{\mathrm{s}} + 965.9 \ (\mathrm{kg/m^3}) \tag{S6}$$

$$\lg(\mu_{\mathrm{HOA}}) = -0.000022 T_{\mathrm{s}}^2 - 0.0290 T_{\mathrm{s}} + 8.187 \ (\mathrm{Pa \cdot s}) \tag{S7}$$

$$\lg(\mu_{\mathrm{OCT}}) = 0.000013 T_{\mathrm{s}}^2 - 0.0166 T_{\mathrm{s}} + 4.372 \ (\mathrm{Pa \cdot s}) \tag{S8}$$

$$C_{\mathrm{pHOA}} = 4.036T_{\mathrm{s}} + 802.2 \ (\mathrm{J/(kg \cdot K)}) \tag{S9}$$

$$C_{\mathrm{pOCT}} = 0.0078T_{\mathrm{s}}^2 - 2.0684T_{\mathrm{s}} + 2035 \ (\mathrm{J/(kg \cdot K)}) \tag{S10}$$

$$k_{\mathrm{HOA}} = 1.69 \times 10^{-7} T_{\mathrm{s}}^2 - 3.89 \times 10^{-4} T_{\mathrm{s}} + 0.2388 \ (\mathrm{W/(m \cdot K)}) \tag{S11}$$

$$k_{\mathrm{OCT}} = 3.069 \times 10^{-4} T_{\mathrm{s}} + 0.1113 \ (\mathrm{W/(m \cdot K)}) \tag{S12}$$

$$k_{\mathrm{q}} = 0.0013T_{\mathrm{q}} + 0.9767 \ (\mathrm{W/(m \cdot K)}) \tag{S13}$$

where superscript HOA represents oleic acid and OCT represents 1-octadecene or octodecane. The temperature unit is Kelvin. The following mixing rules were used to calculate the density, viscosity, heat conductivity and heat capacity of the mixture of HOA and OCT, according to the basic knowledge of chemical engineering principle.

$$1/\rho = w/\rho_{\mathrm{HOA}} + (1-w)/\rho_{\mathrm{OCT}} \tag{S14}$$

$$\lg(\mu) = x\lg(\mu_{\mathrm{HOA}}) + (1-x)\lg(\mu_{\mathrm{OCT}}) \tag{S15}$$

$$C_{\mathrm{p}} = wC_{\mathrm{pHOA}} + (1-w)C_{\mathrm{pOCT}} \tag{S16}$$

$$k = yk_{\mathrm{HOA}} + (1-y)k_{\mathrm{OCT}} \tag{S17}$$

where w is the mass percentage of oleic acid, x is the molar percentage of oleic acid, and y is the volume percentage of oleic acid.

The geometry for simulation was shown in Figure S2(a), where a 2D axial symmetry model was applied to show the 3D structure. The 1 mm diameter solution was surrounded by 1 mm thick quartz, which length was 20 mm. The inlet of the fluid was set to the parabolic velocity distribution u = f (r), as shown by Equation S18

$$u = \mathrm{f}(r) = u_0\left(1 - \frac{r^2}{R^2}\right) \tag{S18}$$

R = 0.5 mm. The fluid outlet was set to a constant pressure of 0 Pa. The boundary conditions for the heat transfer models are shown in Figure S2(a). Since the oil bath was strongly stirred and the cooling air around the quartz tube flew quickly during the experiment, we directly set a constant temperature for the tube surface, where T_{w} = 255 ºC during heating and 25 ºC during cooling. The temperature of quartz and the solution was equal at the inner surface of the tube. The temperature of incoming fluid was set to a constant value T_0, which was 25 ºC

for heating and 255 ºC for cooling. Other surfaces were set to heat insulation. The 2D model in COMSOL Multiphysics 4.3 has 219,000 tetrahedron gird cells, shown in Figure S2(b), which was dense enough for ignoring the numerical diffusion in calculation. It is difficult to the find differences in results, as higher mesh density was used in calculation. The simulations were implemented by a HP workstation with 2.6 GHz CPU and 16 GB memory. Figure 1(d) in the main text shows the temperature fields, and Figure S2(c-d) shows the velocity and pressure distributions.

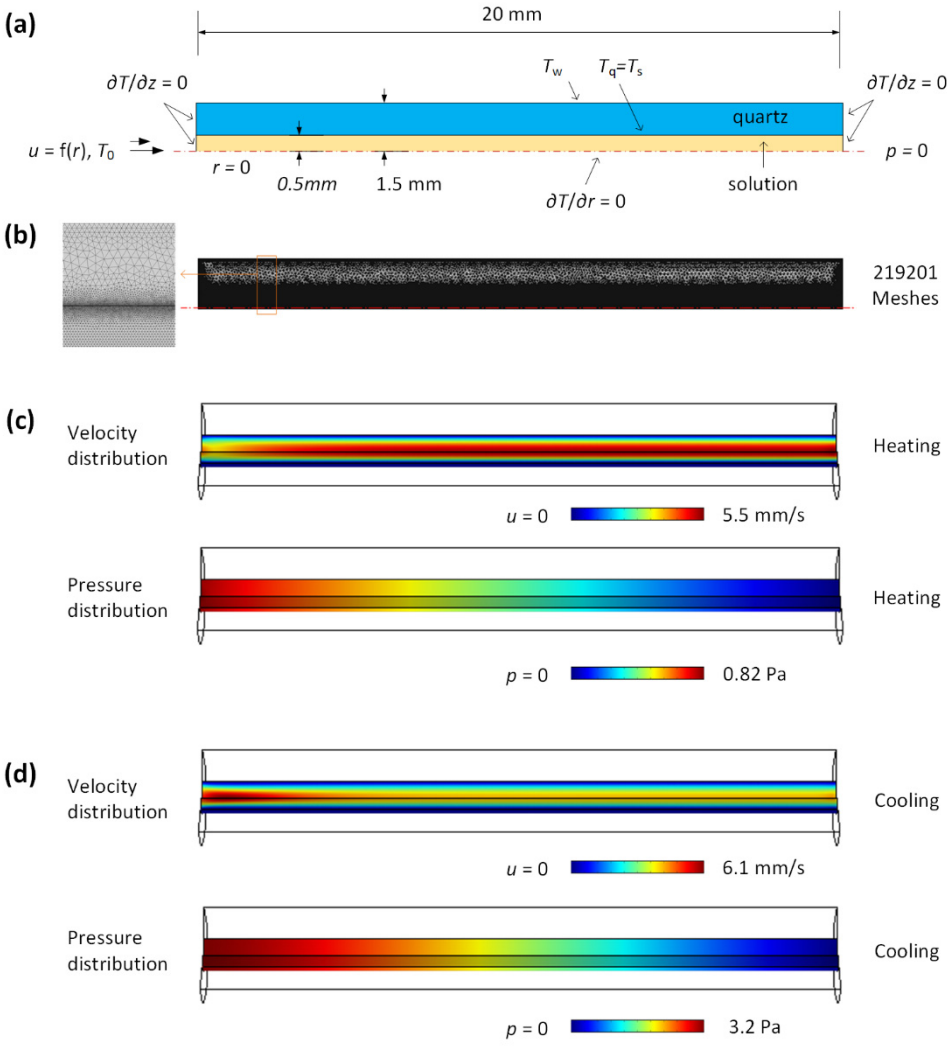

Figure S2. Control and results of CFD simulation

(a) Geometry of the quartz tube and the inside solution. The dashed line at bottom is the axis of symmetry in the 2D model. (b) Meshes in the COMSOL Multiphysics 4.3. (c) Velocity and pressure distributions in the heating tube. (d) Velocity and pressure distributions in the cooling tube. The flow rate controlled by the syringe at 25 ºC was 100 μL/min.

Conversions of the rare earth oleate

To show the effect of precursor solution on the conversion of the rare earth oleate $RE(OA)_3$, we titrated the rare earth (RE) concentrations in the mother liquors with ethylene diamine tetraacetic acid (EDTA) after centrifugally separation of solid particles. Results are listed in Tables S1 and S2.

Table S1. The RE concentration and $RE(OA)_3$ conversion after microreaction.

Precursor solutions	Reaction temperature *T* (ºC)	RE concentration in the mother liquor (mol/L)	$RE(OA)_3$ convertion (%)
PS-A	255	0.0249	37.8%
PS-B	255	0.0226	43.5%
PS-C	255	0.0018	95.5%

Table S2. The RE concentration and $RE(OA)_3$ conversion from the improved microreaction experiment

Reactant solutions	Reaction temperature *T* (ºC)	RE concentration in the mother liquor (mol/L)	$RE(OA)_3$ convertion (%)
NH_4REF_4+NaOA	100	0.0073	81.9%
NH_4REF_4+NaOA	115	0.0062	84.5%
NH_4REF_4+NaOA	135	0.0050	87.5%
NH_4REF_4+NaOA	155	0.0043	89.3%

Surface element analysis of solid products

The surface chemistry of the solids from microreaction experiment using PS-A and PS-B as precursor solutions was analyzed via an ESCALAB 250XI X-ray photoelectron spectrometer (XPS, Thermo Fisher Scientific, Inc.) with Al target as the X-ray source. Figure S3 and Table S2 exhibit that very little RE elements exited on the particle surfaces.

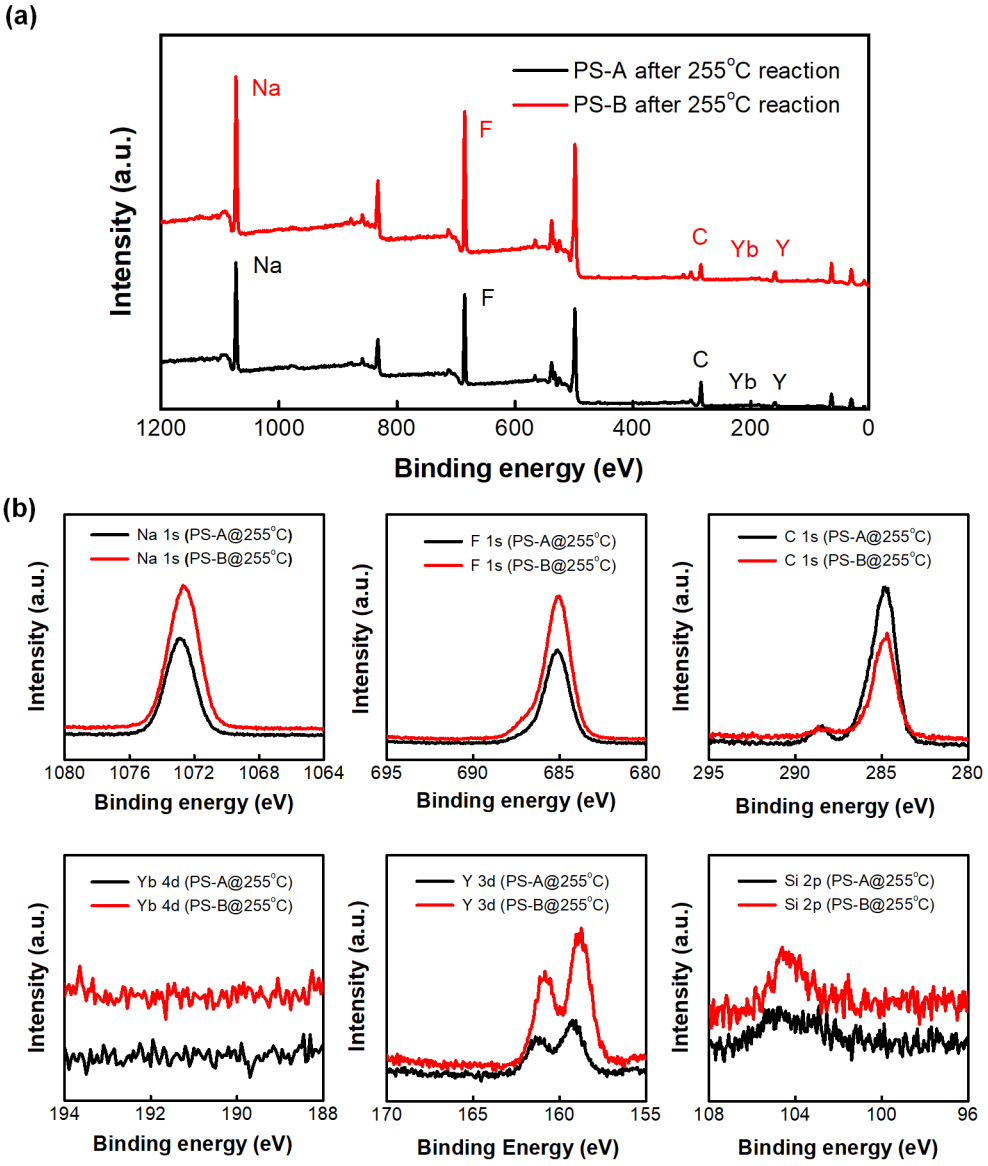

Figure S3. XPS spectra of the solids from 255 °C microreaction experiment.

(a) A general survey; (b) De-convoluted regions of XPS spectrum with their corresponding assignation for each elemental chemistry

Table S3. Surface element compositions.

		PS-A after 255°C microreaction		PS-B after 255°C microreaction	
Element	Electronic orbit	Position (eV)	Atomic (%)	Position (eV)	Atomic (%)
Si	2p	102.9	1.74	104.5	2.22
Y	3d	159.3	1.17	158.8	2.07
C	1s	284.8	32.8	284.8	16.1
F	1s	685.1	37.1	684.7	46.2
Na	1s	1072.9	27.2	1072.3	33.5

The surface chemistry of the solids in the mixture of $RE(OA)_3$ and NH_4F was also analyzed via XPS, which has a detecting depth of 10 nm. The results in Figure 4(d) and Table S4 reveal that the amount of N is roughly the same as Y, and the ratios of F/N and F/Y are close to 4, which imply that the solids could be NH_4YF_4, generated from the reaction between $Y(OA)_3$ and NH_4F.

Table S4. Respective surface element compositions

Element	Electronic orbit	Position (eV)	Atomic (mol%)
Y	3d	158.7	4.97
C	1s	284.8	55.5
N	1s	401.9	5.26
O	1s	537.1	12.2
F	1s	684.8	22.1

Quantum chemistry calculation

To deeply understand the experimental phenomenon, quantum chemistry calculation was carried out to show the free energy variation in the reaction of $RE(OA)_3$ and F^-. The quantum chemistry calculations were performed with DFT technique using the Gaussian 09 D program package. We employed Becke's 3-parameter hybrid functional combined with Lee–Yang–Parr correlation functional (B3LYP) method together with the 6-31G basis set utilizing geometry optimization. Considering the complexity of a long carbon chain, yttrium acetate $Y(Ac)_3$ were employed to simplify the molecule model. Energy-consistent scalar-relativistic WB-adjusted 28-electron core PPs were selected for Y^{3+}. The corresponding basis sets were taken from the basis set library of the Gaussian 09 D program package, namely MWB28. All other lighter atoms were treated at the all-electron (AE) level, and standard 6-31G basis sets. This method is compared by the resolution of the identity second-order Møller−Plesset perturbation theory approach (RIMP2) and has been recognized as a good basis set in the system of rare earths. The electronic energy is calculated as $E = E_T + E_V + E_J + E_{XC}$, where E_T, E_V and E_J are the electronic kinetic energy, the electron nuclear attraction and the electron–electron repulsion terms, respectively. The electron correlation has been taken into account in DFT technique via the exchange correlation term EXC, which includes the exchange energy rising from the antisymmetric quantum mechanical wave function and the dynamic correlation in the motion of individual electrons. Hence it makes DFT dominant over any other conventional procedure. HOMO and LUMO information of corresponding compounds are shown in Figure S4.

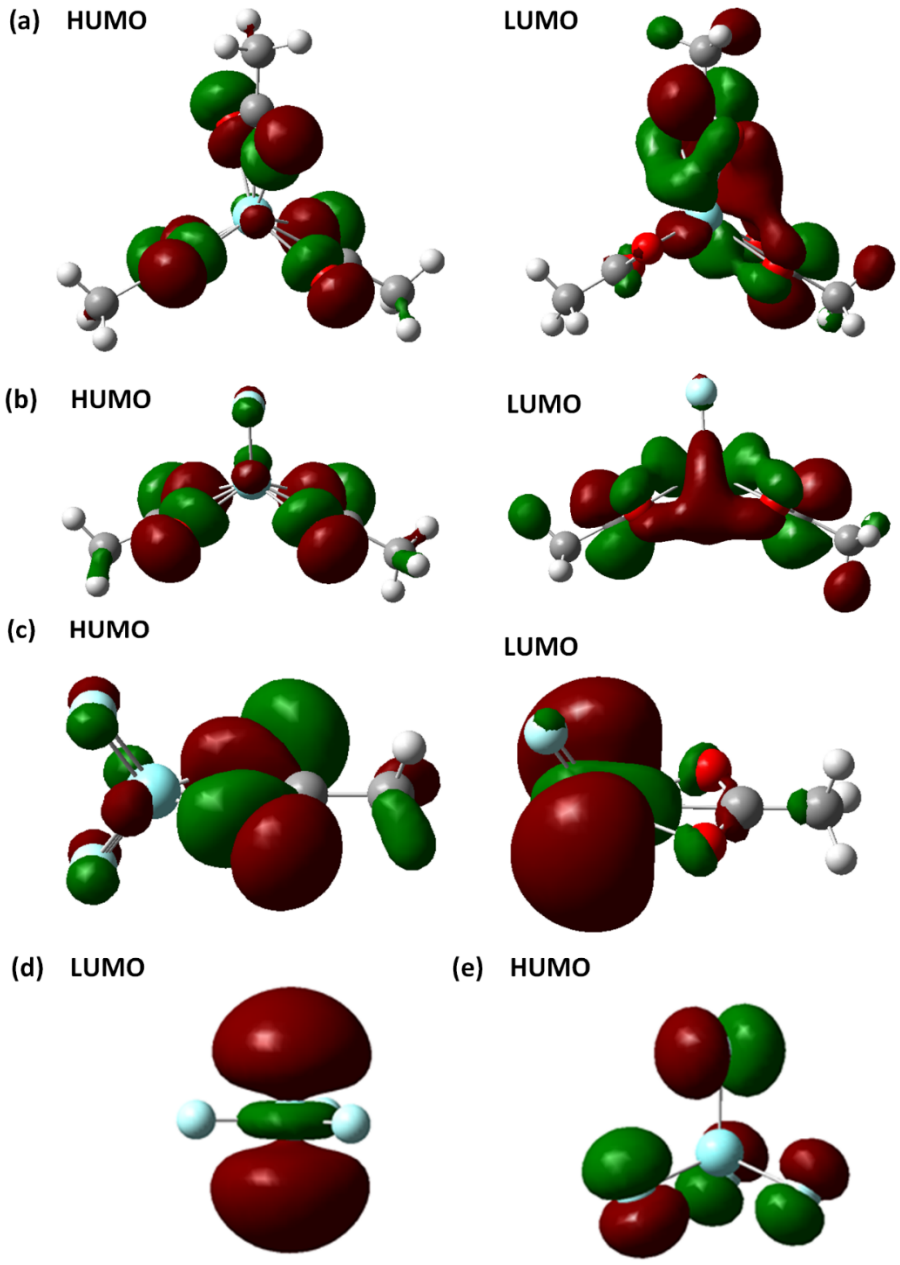

Figure S4. The HOMO and LUMO of $Y(Ac)_3$, $Y(Ac)_2F$ and $Y(Ac)F_2$, YF_3, YF_4^-

(a) $Y(Ac)_3$, (b) $Y(Ac)_2F$, (c) $Y(Ac)_2F$, (d) YF_3, (e) YF_4^-

Size measurement of α and β-$NaREF_4$

Size distributions of the α-$NaYF_4$:Yb,Er nanoparticles from the microreaction experiments were obtained from TEM images. At least 200 particle samples were taken into statistics for each experimental condition. Since the α-$NaYF_4$:Yb,Er particles are not regular in shape, the radial direction of the "nanofiber" assembled by particles was used as the measuring direction, as shown in Figure S5(a). Size distributions of β-$NaYF_4$:Yb,Er and the particle mixture of α and β-$NaYF_4$:Yb,Er from the Ostwald-ripening experiments were also obtained from at least 200 particles in TEM images. For both the elliptical and hexagonal particles, area equivalent diameters are used as the particle diameters, as shown in Figure S5(b).

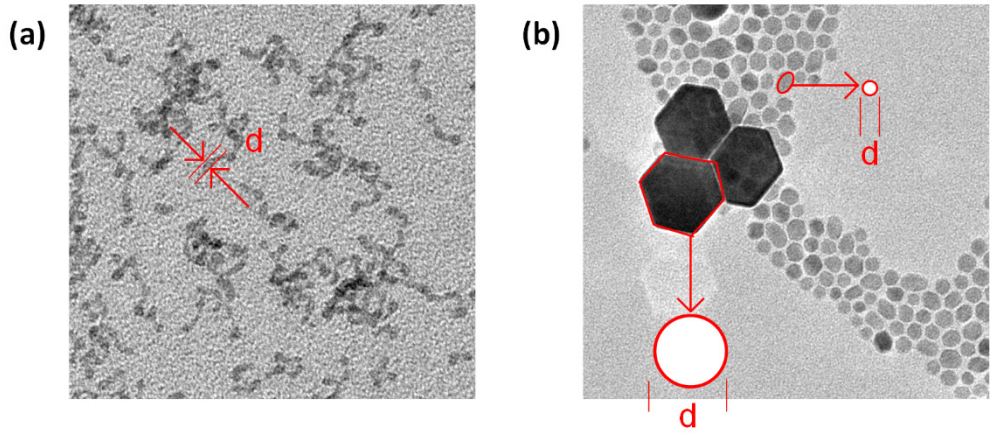

Figure S5. Measurement directions of nanoparticle size

XRD results of the Ostwald-ripening products

The X-ray diffraction (XRD, Bruker, D8 Advance) results in Figure S6 demonstrate that all the solid products from Ostwald-ripening reactions with α-NaYF4:Yb,Er from the improved the microreaction experiments were β-NaYF4:Yb,Er.

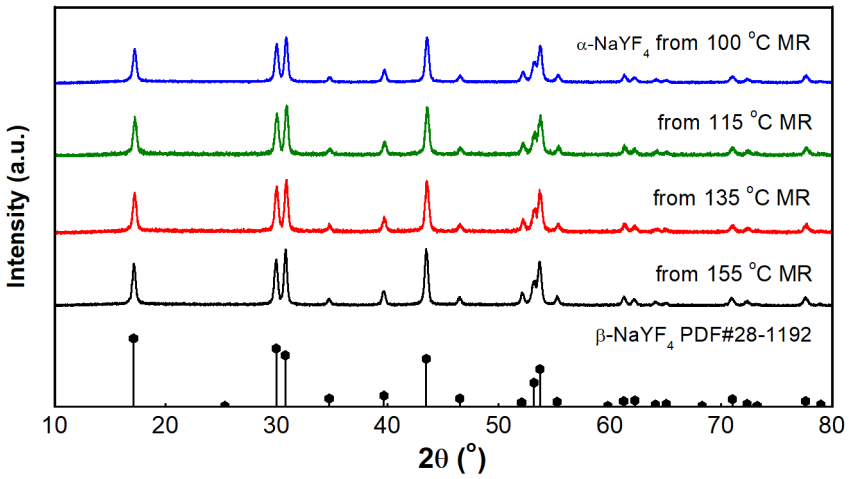

Figure S6. XRD spectra of β-$NaYF_4$:Yb,Er particles after 1 h Ostwald-ripening experiment at 300 °C. The legends show the reaction sources (α-$NaYF_4$:Yb,Er) are from improved micro-reaction experiment with different temperatures.

Luminescence characterization

Upconversion luminescence spectra of β-$NaYF_4$:Yb,Er nanoparticles in their cyclohexane suspensions were detected by a UV-vis spectrometer (USB 2000+, Ocean Optics) equipped with an externally tunable 980 nm infrared diode laser source (Changchun New Industries Optoelectronics Technology Co., Ltd.). The results are shown in Figure S6, which exhibited well green color.

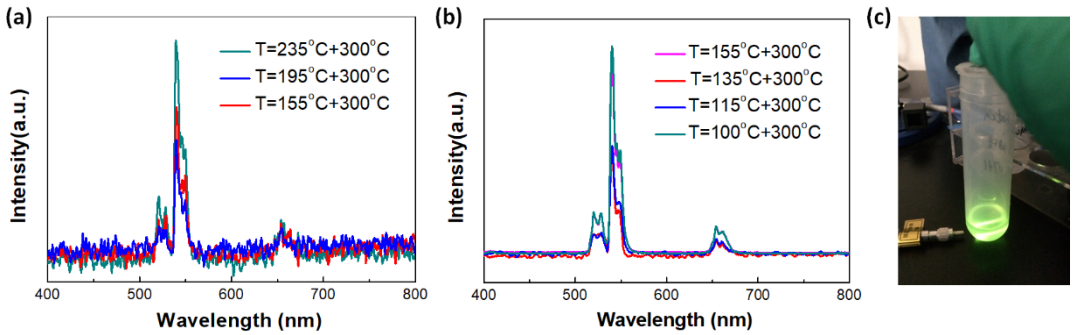

Figure S7. Lightening characterization results of β-$NaYF_4$:Yb,Er

(a) and (b) Upconversion luminescent spectra for the particles in the main text, Figures 6 and 8, respectively. Label T shows microreaction temperature + Ostwald-ripening temperature. (c) A picture of the lightening experiment.

REFERRNCE

1 G.Q. Liu, L.X. Ma, and J. Liu, *Chemistry and chemical property data manual*, Chemical Industry Press, Beijing, 2002.